Chapter 14

Structure-Dependent Biological Response of Noble Metals: From Nanoparticles, Through Nanowires to Nanolayers

Jakub Siegel, Marek Staszek, Markéta Polívková, Michaela Valová, Pavla Šuláková and Václav Švorčík

Additional information is available at the end of the chapter

http://dx.doi.org/10.5772/intechopen.71440

Abstract

Noble metals in their diverse nanoforms bring revolution to many fields of science and technology, as they provide unique properties over their bulk counterparts. Thanks to these completely unprecedented properties, commercial sphere pressure is growing to use them in everyday life. Unfortunately, one of the issues that are subject to dramatic changes is the reactivity of these structures. This may have often fatal consequences to the living organisms. Due to the fact that the mechanism of action of metal nanostructures on living organisms is not yet fully elucidated even in the case of the most studied noble metals such as gold and silver, it is necessary to continue intensively in their research, characterization and categorization. The main prerequisite for the undistorted study of interactions of nanostructures with living organisms is the use of suitable methods of their preparation. Within this context, this chapter attempts to summarize current knowledge form the field of synthesis of metal nanoparticles, layers, wires, and other nanostructures, especially regarding novel techniques of their preparation and extend them by our own results in this area, in the context of their biological properties. More specifically, antibacterial efficacy and potential cytotoxicity of those structures are thoroughly addressed.

Keywords: nanoparticles, nanowires, nanolayers, antibacterials, cytotoxicity, sputtering, noble metals

1. Introduction

This chapter is devoted to the very contemporary themes of polymer nano-metallization, the process giving the polymers exceptional properties in biological applications, namely the bactericidal

action while preserving sufficiently low cytotoxicity level [1–8], as well as to novel techniques for metal nanoparticle (NP) synthesis providing antibacterial, cell-conform entities [9, 10]. So far many efforts has been spent to synthesize the next generation antimicrobial materials applicable in the health-care industry in response to increasing resistance of the pathogens to conventional antibiotics [9–12]. A lot of strategies have been developed to produce those sophisticated man-made materials which hinders their single-key classification. Here, we chose a categorization based on the way of metal incorporation into/on polymer matrix. From this point of view, one can primarily consider the form in which the both components enter the preparation process to form metal-polymer composite. Therefore the composites may be classified into (i) *in-situ* synthesized [13–17]; both polymer and metal are present in reaction chamber in which both components form from their precursors in chemical reaction. Within this protocol, silver nanoparticles have been synthesized in starch-based hydrogels consisting of dissolved N-vinyl pyrrolidone, acrylamide, or acrylic acid dispersed in water. Final polymerization was accomplished by gamma irradiation [13]. Vimala et al. [15] also utilized hydrogels prepared by polymerizing acrylamide with starch and cross-linking agent in the controlled reduction of trapped silver ions by $NaBH_4$. To eliminate toxic borohydrate, which is accompanied by hydrogen evolution, glucose and chitosan have also been used as reducing agents for Ag ions [17]. Reducing mechanism of sugars has been described in detail in Ref. [16]. Another group of composites form (ii) semi *in-situ* synthesized materials; only one component is present in the form of precursor (metals usually precipitate in/on the matrix polymer under the chemical reaction or physical deposition [1–6, 8, 12], whereas polymers are usually heat-treated while the finalized metal nanoparticles are mixed in Ref. [18]). Last group forms (iii) *ex-situ* synthesized composites; both components enter the preparation process until their complete synthesis [4, 19, 20]. The latter mentioned approach generally covers the processes such as grafting, embedding, chemisorption, physisorption, and non-reactive implantation.

In the following text, we attempt to summarize current knowledge form the field of metal nanoparticles, layers, wires, and other nanostructures, especially regarding to novel techniques of their synthesis and extend them by our own results in this area in the context of their biological properties. More specifically, antibacterial efficacy and potential cytotoxicity of those structures are thoroughly addressed.

2. Metal nanoparticles in liquids: preparation fundamentals

Cathode sputtering is a well-established method for the preparation of thin films. It involves bombardment of the target of required composition with energy particles that causes the atoms to be ejected from the target material. These atoms gradually settle on the substrate, where they form a thin layer. Since the whole process takes place under reduced pressure, only solid substrates have been used for a long time. It was not until 1996, when Gao-xiang. et al. [21] tried to prepare a thin layer on a liquid medium by sputtering process. Silicone oil has been chosen as a substrate and it was found that to produce a thin film on this oil is needed to use a power of more than 30 watts. At lower power levels, the layer did not develop and a nanoparticles (NPs) solution was formed instead. Unfortunately, these NPs were not characterized because

the research focused solely on the preparation of the layers [21]. Since then, the research in this area has divided on two streams. The first focuses on the preparation of metallic layers on liquid substrates with their potential use in lunar telescopes [22]. The second one is dealing with the preparation of NPs. The advantage of this method is the ability to prepare NPs without the use of reducing agents and other surfactants. The resulting system typically consists of only two components (1) the liquid substrate used and the (2) nanoparticles formed. As a liquid substrate, any liquid with a sufficiently low vapor pressure can be selected. However, especially for the preparation of NPs, it is desirable that such liquids have the ability to stabilize forming NPs sufficiently. For this reason, ionic [23] or macromolecular [24] fluids are most often chosen. Even a low-molecular glycerol [10] has been documented.

Ionic liquids meet these requirements very well. These liquids consist of an organic cation and an inorganic or organic anion, typically with the melting point below 100°C. The main advantages of ionic liquids is almost zero vapor pressure (e.g. [Bmim]PF6 at room temperature having the vapor pressure of 0.1 nPa [25]), high thermostability, large electrochemical window (range of the voltage at which the substance may be reduced as well as oxidized), fire resistance and in particular solvation properties [26]. For the preparation of NPs, it is also advantageous that ionic liquids generally have a low surface tension which results in a higher nucleation rate and thus NPs of nanometer sizes up to atomic clusters can be prepared [23]. On the other hand, liquid electrolytes are often toxic [27], which is a limiting factor for the subsequent use of produced NPs.

For this reason, toxicologically acceptable macromolecular fluids are used, such as vegetable oils [28], polyethylene glycols (PEG) [29] of different molecular weights and its derivatives [4, 30]. Compared to ionic liquids, macromolecular liquids are characterized by higher vapor pressure (e.g. 0.26 and 0.45 kPa at room temperature for castor oil and soybean oil, respectively [31]) and a worse ability to stabilize NPs [24]. For PEG (and its derivatives), it is highly advantageous to use a PEG of a specific molecular weight, since it directly determines PEG properties, including vapor pressure, stabilization capabilities and also viscosity [32].

An exceptional position between liquid substrates used to prepare NPs by sputtering has glycerol [10]. Compared to previously described substrates, glycerol is naturally biocompatible because it is a fat component in the form of its esters. Another undisputed advantage of glycerol is its frequent use in the cosmetics and soap industries, resulting in both its low production cost and available and well-measured values of all important physicochemical parameters. On the contrary, its disadvantage is substantially higher vapor pressure (22 mPa at room temperature) [33].

Independently on the liquid substrate selection, NPs of different sizes were prepared by sputtering [24]. However, it is apparent from the present results that the resulting NP size is determined primarily by the choice of liquid media. The question, however, remains where the NP is growing in the liquid and how the fluid is involved in this growth. In essence, only three scenarios can occur: (i) NPs nucleation and their growth occur exclusively on the surface of the liquid, (ii) nucleation takes place on the surface of the liquid; whereas the growth itself is already in its volume, and (iii) the sputtered atoms have sufficient energy to penetrate into the volume of the liquid, where both processes (nucleation and growth) take place [34]. In

this case, the penetration depth of the sputtered atoms is the function of their kinetic energy, which may explain the dependence of the final NP size on the deposition parameters. For processes (i) and (ii), the parameters such as working current, voltage, pressure, etc. have only the significance regarding liquid surface saturation velocity. Which of the above-mentioned scenarios will occur depends, according to one part of the scientific community, on the surface and volume composition of the liquid [28], according to others, on the viscosity of the liquid and the vapor tension [35]. Supporters of the first theory assume that after the formation of the nucleus at the liquid/vacuum interface, nanostructures on the surface of the liquid develop, which then diffuse into the volume of the liquid. Here, the nanostructures are self-assembled to the most energy-efficient structure [36]. The second theory is based on the so-called diffusion length, being the maximum length in which the sputtered atoms or the formed nucleus can move. At higher viscosities (lower diffusion lengths), these entities have smaller ability to migrate and the resultant colloidal solution thus contains particles of smaller size and narrower distribution [37].

A more detailed view into the formation mechanism of NPs was provided by Anantha et al. [38]. They describe the process of preparing uniform NPs using a so-called *shared coarsening* model. This model is based on the classical nucleation theory and crystal growth. After the impact of the sputtered atoms on the liquid-vacuum interface (or at a short distance below the liquid surface level), a saturated concentration is quickly reached. Atoms are homogeneously distributed throughout the volume and spontaneous nucleation occurs once the critical concentration is exceeded. In the neighborhood of these nuclei, so-called exclusion zones[1] are created. All sputtered atoms that hit this zone are involved in the growth of the nucleus. Since these zones have a hemispherical shape, secondary nuclei are formed in free space between primary exclusion zones. Subsequently, the primary nucleus grows at the expense of the secondary ones- the *shared coarsening* occurs. When sputtering is terminated at the time of formation of secondary nuclei, the resulting colloidal solution contains uniform NPs. With longer sputtering periods, the particles grow further until they begin to touch each other. This results in change of NPs shape, their agglomeration and the undesirable phenomenon of so-called Oswald ripening takes a place.

Thus, this model considers the sputtering time as one of the most important parameters for the preparation of uniform NPs. This is, however, in direct contradiction with a number of studies that have found the sputtering time not essentially important with respect to size and distribution [39]. This can be explained by the fact that the model published by Anantha et al. [38] does not reflect changes in concentration throughout the whole volume of the liquid. During deposition, the deposited material accumulates at the liquid-vacuum interface (or at a small depth below the surface). Therefore it is clear, that from the very beginning of the deposition the diffusion flow of the emerging NPs will increase, which can be characterized by the first Fick's law for unidirectional diffusion.

$$J_i = -D_i \frac{\partial c_i}{\partial x}, \tag{1}$$

[1]In some literature the term denuded zone instead of the exclusion zone is used.

where J_i means diffusion flux, D_i diffusion coefficient, c_i concentration of sputtered material, and x direction of the flux (in this case the depth of the liquid). Diffusion coefficient in this equation is temperature dependent variable, which can be described for spherical particles by the Stokes-Einstein equation.

$$D = \frac{k_B T}{6\pi\eta r'} \tag{2}$$

where k_B is Boltzman constant, η viscosity of liquid medium, T temperature, and r NP radius. Theoretically, there may be case in which the formed NPs are driven away with diffusion flux J, leave space in the liquid-vacuum interface, where new nuclei and NPs can be formed. In this case, the size distribution of the prepared NPs may not have been deteriorated.

Since the diffusion coefficient is a parameter which dependents also on the viscosity of the medium and the diffusion length, it is obvious that the most important variable in the preparation of NPs by sputtering is the choice of the liquid itself and the temperature during deposition process. Several groups focused on the examination of the dependence of NP size on viscosity of used medium. From **Table 1**, it is apparent, that our research group [40] achieved remarkable results. We successfully controlled the NP size in temperature range 0–20°C with average size change 0.5 nm/°C (see **Figure 1**) [40]. On the other hand, above this range we observed significant evaporation of glycerol. This evaporation influenced the mechanism of formed NPs, resulting in the production of smaller ones. From **Table 1**, it is also apparent, that most pronounced changes were observed on those substrates having a higher viscosity dependence on the temperature. The knowledge gained from this work can be used to study the physicochemical properties of NPs, as they declare the possibility of preparing NPs of the

Temperature	Nanoparticles size [nm]		
	PEG600	C_4mim^+/BF_4^-	PVP-Glycerine
5°C			12.8
10°C			13.1
15°C			15.6
20°C	2.73	0.75	7.2
30°C	3.70	0.70	7.8
40°C	4.67	1.34	
50°C	5.55	2.30	
60°C	7.40	2.76	
70°C		3.24	
80°C		3.61	

Table 1. Dependence of nanoparticle size on temperature in different liquid media: PEG600 ionic liquid [37] C_4mim^+/BF_4^- [35] and PVP-glycerine system [40].

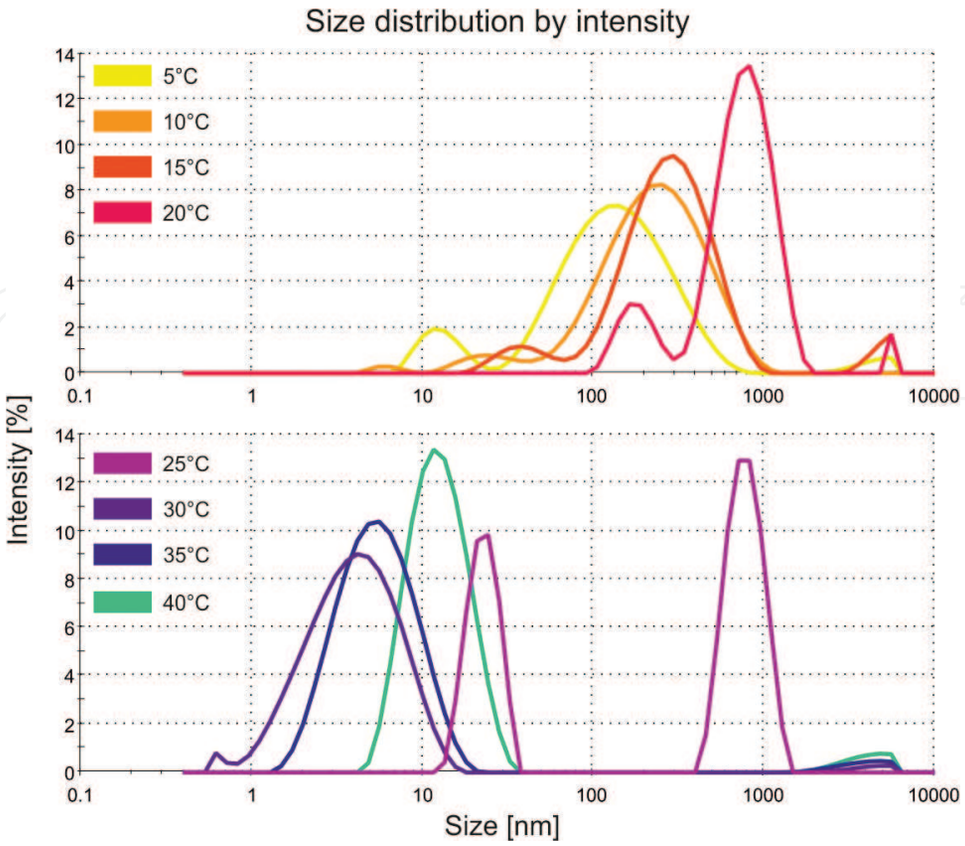

Figure 1. Dynamic light scattering analysis of aqueous solutions of silver NPs prepared at different temperatures of the liquid substrate [40].

desired size, while maintaining a constant environment containing minimal number of components. The whole process of evaluating NPs physicochemical properties is thus simplified, in particular, to the consideration of different environment influence. This is very advantageous, for example, in the detection of potential toxicological properties of these structures. These NP properties must be known very precisely owing to the boom of their use in broad commercial applications and products [41].

3. Nanoparticles cytotoxicity

Currently, there can be found enormous number of scientific papers dealing with NPs toxicity. Unfortunately, despite of the amount of information available, the NP toxicological properties cannot be clearly interpreted, especially the toxic doses. This applies even for the most studied types of NPs – gold and silver ones (see reviews [42, 43]). This fact was considered in our related study [9], addressing NPs biological properties. We used cathode sputtering method to prepare NPs of gold (6.1 ± 1.0 nm), silver (4.2 ± 0.9 nm), palladium (2.5 ± 0.6 nm), and platinum (1.8 ± 0.6 nm). Prepared NP suspensions were further diluted with water for ion chromatography in a weight ratio of 1:3 (glycerol:water). This step is necessary as the isotonicity of the solution is achieved (see **Figure 2**) and the bioassay distortion is avoided. For

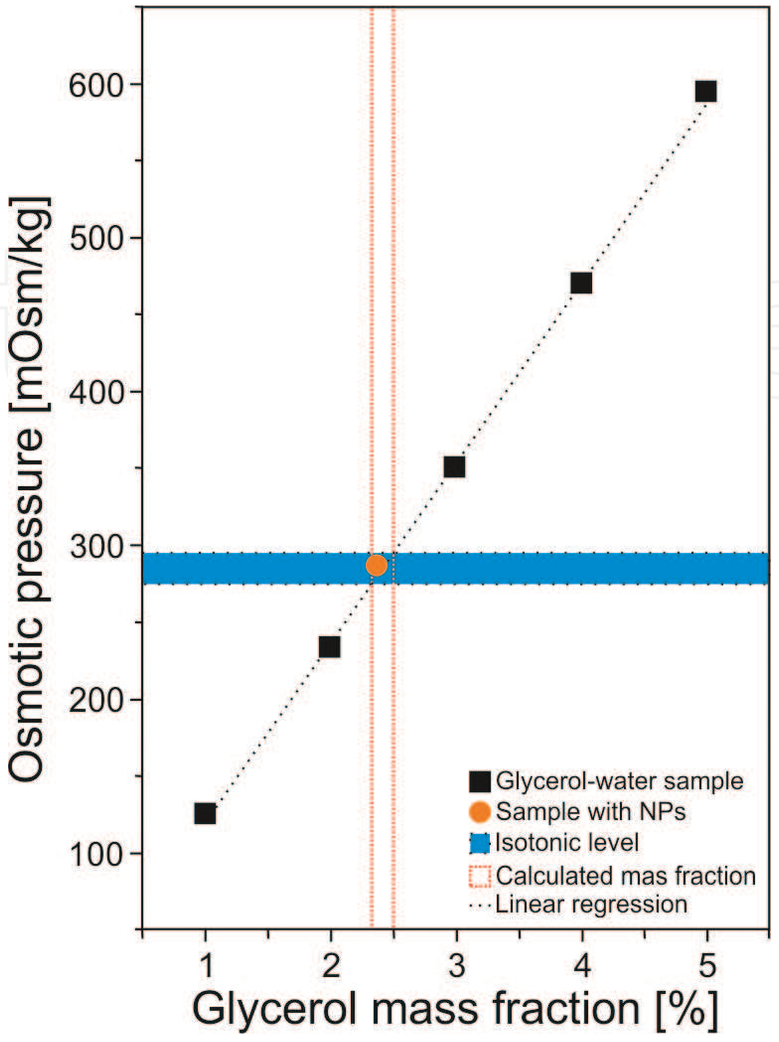

Figure 2. Dependence of tonicity on the composition of solution glycerol:water. The blue band indicates the isotonic environment from which the glycerol:water ratio was calculated by linear regression. The orange dot indicates thus solution enriched with silver nanoparticles.

bioassay purposes, it is also important that our NPs were stabilized electrostatically and not sterically, in contrary to most published results of other scientific groups [44, 45], thus avoiding further bioassay distortion caused by surfactants side-effects. Prepared colloidal solutions were then subjected to various cell lines via WST-1 assay. More specifically, the NPs were tested against A549 (human lung carcinoma cells), HaCaT (human keratinocytes), RAW 264.7 (mouse macrophages), CHO-K1 (Chinese hamster ovary), NIH 3 T3 and L929 (both mouse embryonic fibroblasts), the cell lines commonly used to evaluate the cytotoxic potential of pollutants [24]. The cytotoxic potential was investigated for 24, 48 and 72 h over the NPs concentration range of 0–6.150 mg/ml [9].

Figure 3 illustrates the results obtained for L929 cell line. The differences in absorbance values on y-axis directly correlate with the formation of formazan, which is metabolized by viable cells. In **Table 2**, all results are summarized in the form of the half maximal inhibitory concentration (IC50). It obvious, that the highest toxicity was observed in case of Pt and Pd

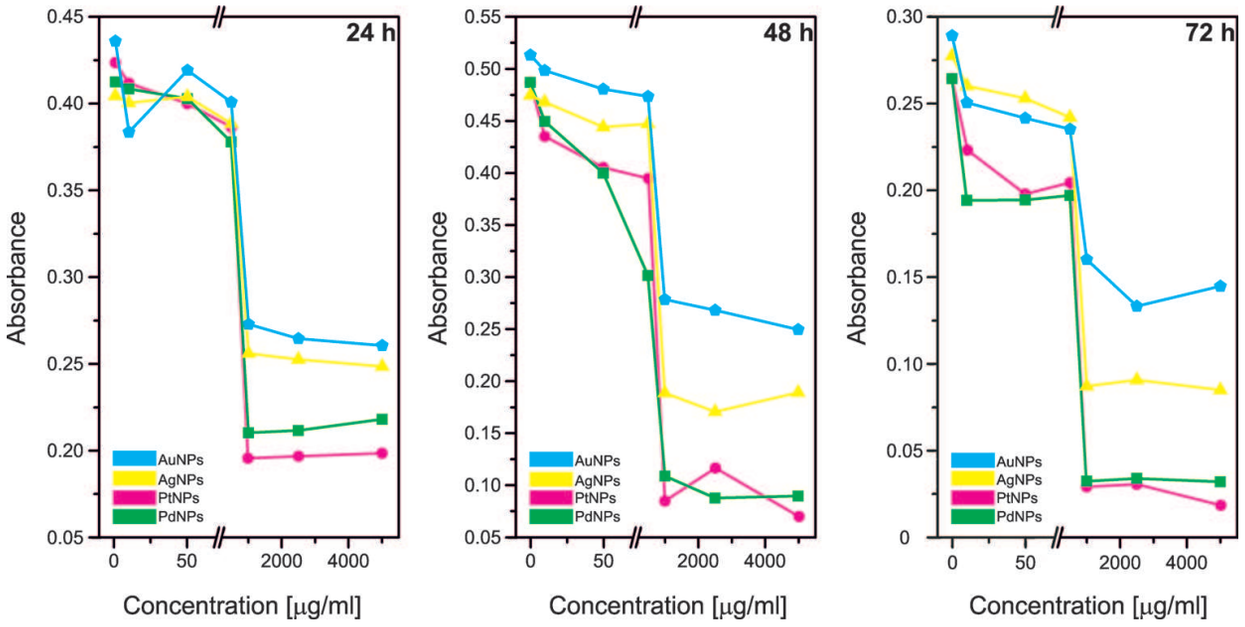

Figure 3. Cytotoxicity of Ag, Au, Pd, and Pt nanoparticles on L929 cells after 24, 48 , and 72 h of treatment.

nanoparticles, less for Ag and almost no toxicity for Au NPs. These results are partially consistent with the findings of Asharani et al. [46], who examined the cytotoxic potential of Ag NPs (5–25 nm), Au NPs (15–35 nm), and Pt NPs (3–10 nm) on the zebra fish embryos. In their work, the cytotoxicity of the gold nanoparticles was not observed, and the mortality rates for Ag NPs and Pt NPs (at concentrations of 100 mg/ml) were determined to 30 ± 12.8% and 50 ± 9.9%, respectively. It is interesting that Ag [46] and Pt NPs [47] are generally reported as highly cytotoxic, while Au NPs [46, 48] are usually considered as biocompatible. This inconsistency with the above-mentioned works can be due to both, different sizes of prepared NPs and the preparation process itself. In referred study [46], authors used a reduction synthesis for preparation of NPs, so the resulting colloids might contain toxic entities such as chlorine

Cell line	IC_{50} [µg·ml $^{-1}$] for 72 h			
	AgNPs	AuNPs	PdNPs	PtNPs
HaCaT	2,250	1,970	1,060	1,010
Hep G2	2,075	3,900	1,425	908
CHO-K1	1,840	2,300	920	855
L929	1,710	1,900	900	770
NIH 3T3	820	1,190	425	550
RAW 267.7	1,580	1,370	880	960

Table 2. The IC_{50} values for individual cell lines after 72 h of treatment with the tested nanoparticles. IC_{50} represents concentration, which causes 50% reduction of cell viability measured by WST-1.

anions, PVA, etc. Authors, despite of their attempt to transfer NPs to the aqueous solution by centrifugation, do not declare the purity of colloid solution before the evaluation of the biological properties. Therefore, the comparison of our results with the above-mentioned work (but also others, e.g. [42]) is rather difficult. In addition, the NP surfactants can cause a dramatic change in their potential toxicological behavior, which remains a challenge to most of works dealing with such type of NPs.

4. Metal-based treatment of polymers

Nowadays, an investigation of non-conventional antibiotic treatment of polymeric medical devices consists from various ways. One of the effective approaches is antibacterial-active biocompatible polymers, where their applications are gentle and safe. One can distinguish two types of antibacterial polymers: (i) polymers which exhibit antibacterial efficacy by themselves and/or (ii) their antibacterial properties are acquired by their controlled modification [49].

In the first case, one can converse natural or synthetic polymers and co-polymers with charged active groups, for example, biguanides, quaternary ammonium, pyridinium, or phosphonium salts [50–52]. The second group represents antibacterial-treated polymers, which achieved their antibacterial activity by adding of organic and/or inorganic antibacterial agents in various manners, such as (i) by incorporation into polymeric matrix or (ii) formation of antibacterial coatings on polymeric surface. Their efficacy is then two-step; their presence on the polymeric surface ensure the reduction of initial bacterial adhesion and thereafter deactivation of already adherent bacterial colonies [53].

In recent days, all of above-mentioned ways of treatment are still developing areas, which produce materials with excellent antimicrobial capability. However, one of the most promising areas in this regard is nanotechnology. Nanostructured noble metals, either incorporated or forming coatings, exhibit strong antibacterial activity against broad spectrum of microorganisms, where bacterial resistance is missing [5, 54–56]. Therefore, in the further text we are focusing our interest on a group of nanostructured noble metals, especially coating-forming ones. This type of surface modifications of biocompatible polymers might not only provide significant antibacterial protection, but also enhance biocompatibility of the resulting composites.

The enhancements of material biocompatibility and antibacterial efficacy by the modification of surface morphology have been referred in several studies [1, 5, 8, 57–59]. Generally, to enhance the functionality of polymeric materials, the formation of nanostructured thin films on its surface might be an effective way. Moreover, one can prepare nanostructured coatings with increased surface area using nanolayers (thin films) as default structures, by their thermally induced transformation into island-like structures. Such increase of surface area often leads to the enhancement of resulting antibacterial response. The formation of island-like structures by low temperature annealing of thin films has been described for silver [5], palladium [8], and gold [57]. Another way to increase the specific surface area and roughness of antibacterial coating is laser patterning of polymeric surface prior to metal deposition, which

leads to the formation of ordered nanowire arrays [1]. This method usually provides better adhesion and proliferation of human cells; at least at those which prefer rougher substrates [58]. Thus, the surface modification enables a direct control over the material biocompatibility, which might be significantly enhanced [59].

In this subsection, we present three types of metal (Ag and Pd) nanostructures; nanolayers (NLs), islands (NIs), and wires (NWs), supported on biocompatible polymer polyethylene naphthalate (PEN), and discus the influence of surface morphology/roughness change (unlike pristine PEN) on their resulting biological response. Surfaces of all used materials were thoroughly characterized by X-ray photoelectron spectroscopy (XPS), focused ion beam cut - scanning electron microscopy (FIB-SEM), and atomic force microscopy (AFM). Thereafter, the biological testing of the samples was accomplished. Antibacterial properties were examined using Gram-negative bacteria *Escherichia coli* (*E. coli*) and Gram-positive *Staphylococcus epidermidis* (*S. epidermidis*), which commonly cause hospital-acquired infections related to biofilm formation due to long-term applications of catheters and other medical devices. Finally, cell-conformity study of all types of composites was carried out using mouse embryonic fibroblasts (L929) as a routinely used cell line for this purpose.

4.1. Preparation of metal nanostructures

Metal (Ag and Pd) coatings on polyethylene naphthalate were prepared by DC sputtering. For a calibration of sputtering device, sputtering times on a glass substrate, simultaneously coated with PEN samples, varied from 10 to 200 s. Effective thicknesses of metal layers were determined by AFM scratch method. To produce island-like structures with increased antibacterial-active surface area, prepared samples were annealed in air atmosphere at 250°C for 1 h, then cooled down in air and stored under laboratory conditions. In this work, we present samples with 20 nm thick Ag and Pd layers (sputtering time 200 s, 20°C, current of 15 mA, total argon pressure of 5 Pa, and electrode distance of 50 mm) and corresponding annealed ones as representatives.

The combination of polymer laser pre-treatment and metal vacuum evaporation was used for the preparation of self-organized, fully separated Ag and Pd NW arrays of the thickness of 20 nm. To prepare periodic nanostructures (ripples) on PEN surface, PEN samples were treated by KrF excimer laser (6000 laser pulses, laser fluence of 10 $mJ \cdot cm^{-2}$). Then, laser-patterned (rippled) PEN was used as a template for Ag and Pd NW arrays (thickness of 20 nm) prepared by vacuum evaporation under the glancing angle of $\phi = 70°$. The thickness of metal NWs was monitored *in-situ* by quartz crystal microbalance during the vacuum evaporation process, and verified by FIB-SEM analysis and AFM scratch test of metal simultaneously deposited on a glass substrate.

Due to the experimental set-up of vacuum evaporation process [the glancing angle (ϕ) of 70°] the formation of metal NWs took place preferably from one side of rippled PEN (for graphical representation see [1]). Mild ripples´ structure is in a correlation with the glancing angle of incidence (so-called shadow effect). The shadow effect modulates the spatial distribution of metal flux and induces the nucleation of metal mainly near to the tops of the illuminated ridges and NWs are formed from one side of the ripples (the highest metal flux) [60]. As the

thickness of the metal coating of polymer increases, the agglomeration and coarsening of the metal clusters increases until a polycrystalline array of metal NWs is formed [61]. This phenomenon was verified by FIB-SEM (see **Figure 4**) and has already been observed also for Au NWs arrays supported on PET [62, 63].

4.2. X-ray photoelectron spectroscopy (XPS)

For the determination of atomic concentrations of elements in metal NLs and NIs, X-ray photoelectron spectroscopy (XPS) analysis was performed under the electron take-off angle of 0° (**Table 3**). In case of metal NWs, the electron take-off angle was 0 and 81°, from which samples were analyzed from both sides; left and right (**Table 4**, for graphical representation see [1]). The analytical information about the chemical composition from the perpendicular direction to the surface (0°) originates from greater depth (8–10 atomic layers), compared to the electron take-off angle of 81°, which provides information just from 1 to 2 atomic layers [1, 64]. The presence of C and O is given by the stoichiometry of polyethylene naphthalate, and might be extended by the hydrocarbon impurities, which are often adsorbed on the surfaces of the polar polymeric materials from air [65]. Detected Ag, in case of Ag-coated samples, and Pd, in case of Pd-coated ones, comes from the process of DC sputtering (NLs, NIs) and vacuum evaporation (NWs).

The results for metal NLs and NIs (**Table 3**) indicated that annealing of pristine PEN caused no significant changes in chemical composition of polymer. Due to diffusion and aggregation of metal during annealing, detected concentrations of metal for annealed Ag (Ag NIs/PEN) and Pd (Pd NIs/PEN) samples were lower, compared to as-sputtered ones (both, Ag and Pd NLs/PEN). However, observed decrease was at the expense of the concentrations of elements originating from the underlying polymer, where underlying polymer become partially uncovered. In the light of the results of surface ablation (XPS) and metal release (ICP-MS) [1], however, we attribute these compositional changes not only to the coalescence of metal into separate NIs, but also to embedding of these clusters into the polymer interior. This ultrathin (ones of nm) surface incorporation was probably caused by polymer overlay reaching almost the tops of individual metal islands (so-called "curtain" effect, for graphical representation

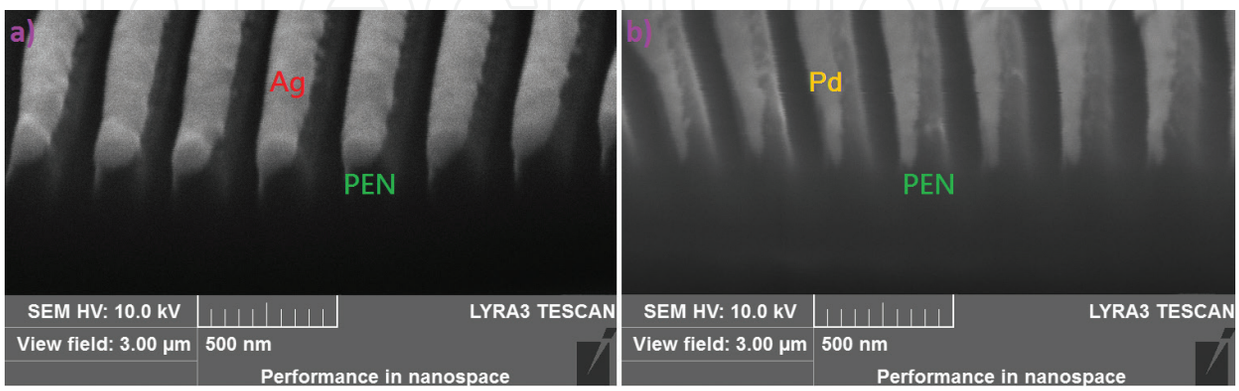

Figure 4. FIB-SEM images of (a) silver and (b) palladium NW arrays supported on laser-patterned PEN.

Sample	Atomic concentrations of elements (at. %)			
	C	O	A g	Pd
pristine PEN	72.2	27.8	-	-
annealed PEN	73.1	26.9	-	-
Ag NLs/PEN	58.4	12.0	29.6	-
Ag NIs/PEN	61.5	30.1	8.4	-
Pd NLs/PEN	73.5	1.2	-	25.3
Pd NIs/PEN	65.6	18.3	-	16.1

Table 3. Atomic concentrations of C(1s), O(1s), Ag(3d), and Pd (3d) for both, pristine and rippled PEN, Ag and Pd/PEN composites measured by XPS, electron take-off angle of 0°.

see [8]). The relatively high value of the atomic concentration of O for the annealed sample coated by Ag (Ag NIs/PEN) could be explained by higher propensity of this sample to oxidation during annealing.

The results for metal NWs are shown in **Table 4**. Unlike the work of Tuma et al. [66], in which a two-step deposition of silver was performed and a dramatic increase of at.% of Ag from the

Angle (°)	Sample	Atomic concentrations of elements (at. %)			
		C	O	Ag	Pd
0	pristine PEN	72.2	27.8	-	-
	rippled PEN	74.4	25.6	-	-
	Ag NWs/PEN	67.7	12.9	19.4	-
	Pd NWs/PEN	80.2	13.4	-	6.4
81 left	pristine PEN	73.0	27.0	-	-
	rippled PEN	79.3	20.7	-	-
	Ag NWs/PEN	63.1	12.1	24.8	-
	Pd NWs/PEN	62.1	12.0	-	25.9
81 right	pristine PEN	73.1	26.9	-	-
	rippled PEN	79.5	20.5	-	-
	Ag NWs/PEN	75.9	15.5	8.6	-
	Pd NWs/PEN	74.4	16.6	-	9.0

Table 4. Atomic concentrations of C(1s), O(1s), Ag(3d), and Pd(3d) for both, pristine and rippled PEN, Ag and Pd NWs/PEN samples measured by XPS; electron take-off angle of 0 and 81° from left and right side of samples.

right side after the second deposition for Ag nanostructures on laser-patterned poly(methyl) methacrylate was observed (18.7% from the right, left 8%), in this work, one-step deposition of metal (Ag or Pd) was used. The results revealed higher values of the atomic concentrations of both, Ag and Pd, from the left side (24.8% from the left, right 8.6% in case of Ag, 25.9 and 9.0% for Pd, respectively). The difference between our and Tumas' results, however, originates only from the rotation of samples during the analysis. The results for the electron take-off angle of 81° from the left and right side for the individual samples of pristine and laser-patterned PEN, showed undistinguishable differences in the atomic concentrations of elements. However, the measurements of metal/polymer composites under the same electron take-off angle revealed above-mentioned significant differences in the concentrations of metal, in case of both, Ag and Pd samples, which verified well the formation of NWs only from the one side of the ripples, which is in well accordance with above-mentioned shadow effect. The different results observed between the samples of pristine and laser-patterned PEN, particularly evident for the electron take-off angle of 81° (both left and right arrangement), were given by the change in the chemical-compositional arrangement caused by the exposure of a laser beam, which is associated with the change of the samples´ surface morphology, evident from atomic force microscopy (AFM) images (see **Figure 6**).

4.3. Atomic force microscopy (AFM)

Because the surface morphology of material has a great impact to its biocompatibility, AFM analysis was employed, too (see **Figures 5** and **6**). The surface morphology of the samples was characterized by surface roughness (R_a) measurements and three-dimensional AFM scans. **Figure 5** shows metal NLs and NIs/PEN composites, **Figure 6** metal NWs/PEN composites.

In **Figure 5**, one can see that the surfaces of pristine PEN and as-sputtered samples (both Ag and Pd NLs) were mildly corrugated with practically the same value of surface roughness. No significant morphology changes were observed after annealing of pristine polymer. However, one can see a remarkable change of the surface morphology of metal-coated samples after annealing (see differences between Ag and Pd NLs/PEN and Ag and Pd NIs/PEN); the annealing caused a complete rearrangement of the surface. Thermal accumulation in metal coating resulted in changes in the amorphous phase of PEN (T_g^{PEN} = 120°C). As the metal coating become rough, noticeable increase of R_a appears; cca two orders of magnitude higher compared to as-sputtered ones (NLs). After the annealing, one can observe the transformation of continuous metal coatings into isolated nanoislands homogeneously distributed over the PEN surface in case of both, Ag and Pd NIs samples. This phenomenon is in accordance with the results of XPS measurements (see **Table 3**); the values of atomic concentrations of metal (both, Ag and Pd) after annealing were decreased at the expense of C and O originating from PEN. Moreover, size and shape of metal NIs might be effectively controlled by the thickness of coating preceding the annealing process [8]. As mentioned above, the formation of island-like structures should lead to the increase of antibacterial-active surface area, resulting in enhanced antibacterial efficacy [5, 8, 57]. However, in this case, annealing resulted in above described "curtain" effect; partial covering of metal nanoislands by thin PEN layer (see Section 4.2. XPS). Based on these results, one can expect rather lower antibacterial efficacy than in case of NLs.

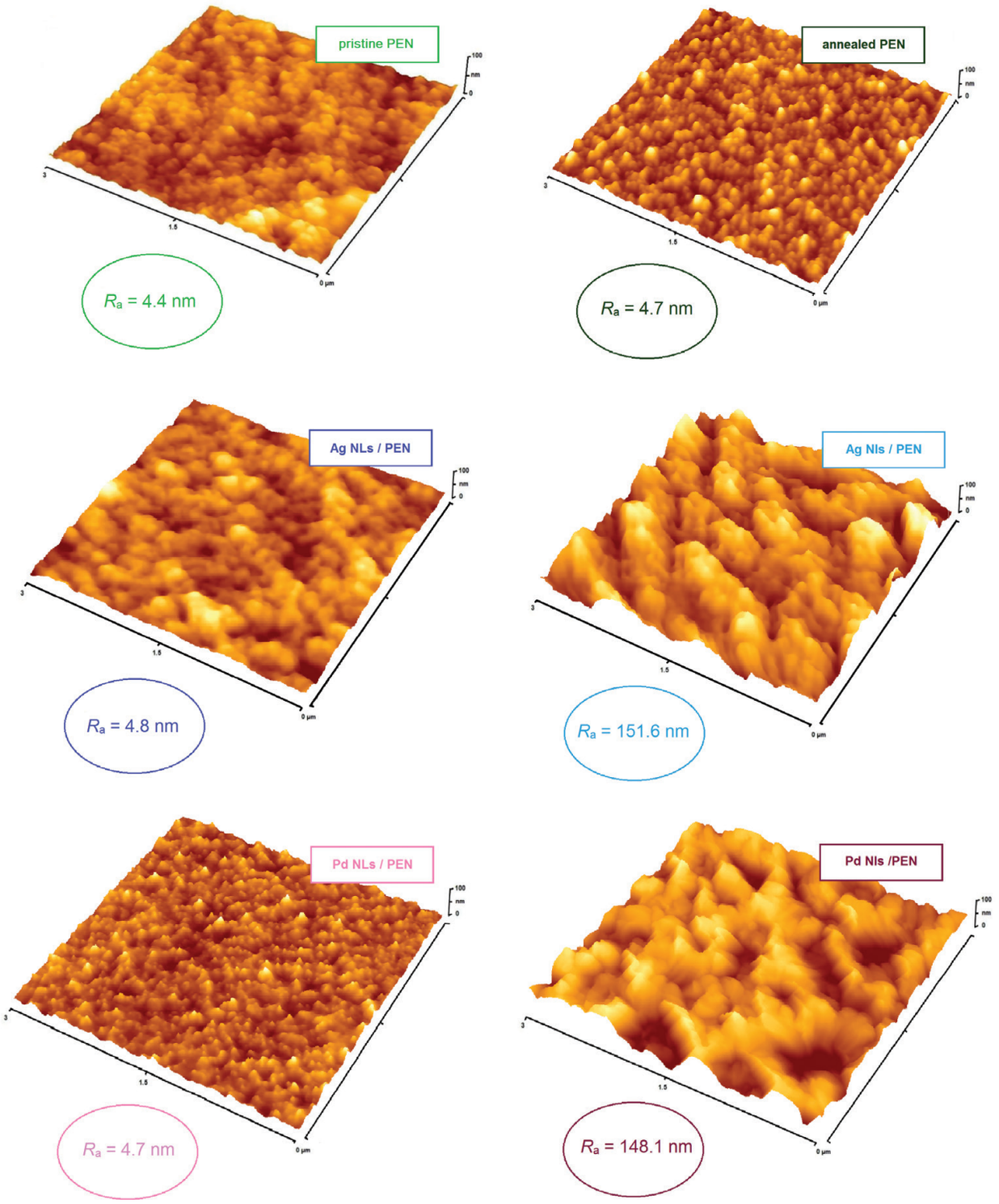

Figure 5. AFM images of PEN, both before (pristine) and after (annealed) annealing, Ag and Pd/PEN composites, together with their surface roughness (R_a).

The results of AFM analysis of metal NWs samples, both Ag and Pd (**Figure 6**) corresponds to FIB-SEM ones (see **Figure 4**), however, FIB-SEM analysis, by which, for example, the distribution and shape of nanowires might be evaluated, is more informative; AFM scans cannot provide the

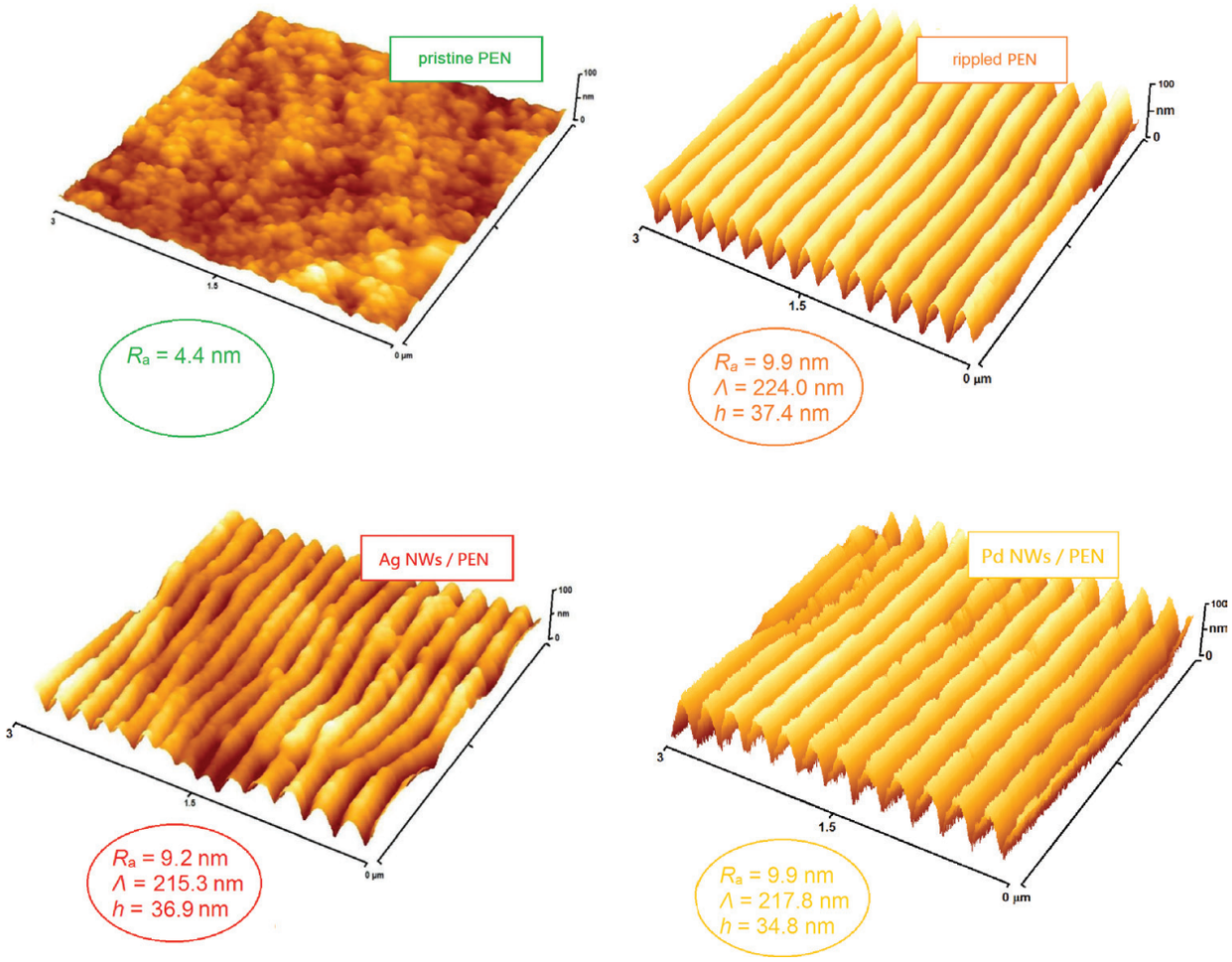

Figure 6. AFM images of PEN, both before (pristine) and after (rippled) laser patterning, Ag and Pd/PEN composites, together with their surface roughnesses (R_a), periodicities (Λ), and heights (h).

imaging of fully separated metal NWs. Using FIB cuts, one can observe the interface between a polymeric substrate (PEN) and metal (see **Figure 4(a)** and **(b)** for Ag and Pd NWs, respectively) and, in case of the analysis of the samples having various thicknesses of NWs, as in the work of Siegel et al. [62], it is also possible to distinguish significant differences between the prepared structures. Surface modification of polymer, such as laser patterning discussed in this paragraph, enables a direct control over the material biocompatibility; significantly increases the adhesion and proliferation of human cells on artificial substrates, and the resulting biocompatibility of material might be effectively enhanced [59]. One of the most important parameter of surface morphology, which has a great impact on the biocompatibility of material, is its surface roughness, which also plays an important role in its resulting antibacterial effects. For example, nanoscale surface roughness was effective to reduce plaque colonization on titanium implants [67]. Thus, the increase of biocompatibility and antibacterial effects of nanometal/polymer composites by laser patterning gives a convenient combination of materials´ properties for their applications in medicine and health-care industry. Regarding to this, we summarized surface morphology and roughness (R_a) of all prepared samples, including the parameters such as periodicity (Λ) and height (h) of nanostructures in case of ripples and wires. **Figure 6** shows self-organized and

well-separated periodic ripples homogenously distributed over the PEN surface. The value of R_a was considerably increased after laser patterning (4.4 nm for PEN and 9.9 nm for PEN ripples). There were no significant differences observed after metal deposition (9.2 nm for Ag and 9.9 nm for Pd, respectively). The values of periodicity and height of Ag NWs/PEN (Λ = 215.3 nm, h = 36.9 nm) and Pd NWs/PEN samples (Λ = 217.8 nm, h = 34.8 nm) were mildly decreased compared to patterned PEN (PEN ripples) sample (Λ = 224.0 nm, h = 37.4 nm), which was probably caused by a partial filling of the ripples by metal during vacuum evaporation process.

4.4. Antibacterial properties

Antibacterial effects of the samples related to control ones (physiological solution) are shown in **Figure 7** for metal NLs and NIs/PEN composites and in **Figure 8** for NWs/PEN composites, both Ag and Pd, in which two environmental bacterial strains (a) Gram-negative *E. coli* and (b) Gram-positive *S. epidermidis* were studied. The samples were examined in both, static and dynamic (shaking at 130 rpm) mode at 24°C (*E. coli*) and 37°C (*S. epidermidis*) for 3 and 24 h of incubation by the drop plate method [68]. After overnight incubation on agar plates, the number of colony forming units (CFU) of each strain was counted. The experiments were accomplished under sterile conditions.

In **Figure 7**, generally, one can see no antibacterial effects of pristine and annealed PEN, except insignificant effect in case of annealed sample cultivated for 3 h in dynamic mode with *E. coli* (**Figure 7(a)**). This phenomenon which might due to rougher surface morphology of this sample (see **Figure 5** AFM), which, together with shaking in dynamic mode, might cause this mild inconformity for bacterial colonies in short period of time (3 h) during which they accustom to surrounding environment [69]. Thereafter, one can observe generally increasing antibacterial effects with incubation time for all composites and treatment conditions, which is in correlation with (i) increasing concentration of released metals into physiological solution with time and (ii) longer contact of bacterial strains with the surface of antibacterial-active-coated samples, both Ag and Pd. For details, see ICP-MS results [8]. When comparing the results of NLs and NIs coatings in case of both metals, one can reveal that metal NLs/PEN samples exhibited similar or higher antibacterial response than NIs ones, which is in accordance with XPS results (see **Table 3**) and data published elsewhere [8], which attributed this behavior to so-called "curtain" effect; metal islands partially covered by thin polymer film. Thus, in the case of PEN, the change of surface morphology induced by annealing did not lead to increased antibacterial activity. When compared to the results for Ag and Pd samples, more significant antibacterial efficacy was observed for Pd ones, in case of both, NLs and NIs/PEN composites. It outlines that Pd nanostructures might be used as more effective alternative of the most commonly used Ag [70–72] for antibacterial coating of medical devices. The differences between the results in **Figure 7(a) and (b)** showed that *S. epidermidis* (**Figure 7(b)**) was more sensitive to both metals compared to *E. coli* (**Figure 7(a)**); the most striking is a total inhibition (no countable amount of CFU) in both modes and incubation times for Pd samples, both NLs and NIs. These different results for different bacterial strains might be explained by generally accepted phenomenon about different composition of their cell walls; positively charged particles of noble metals then more facile penetrate through the cell walls of Gram-positive bacteria (*S. epidermidis*) [73].

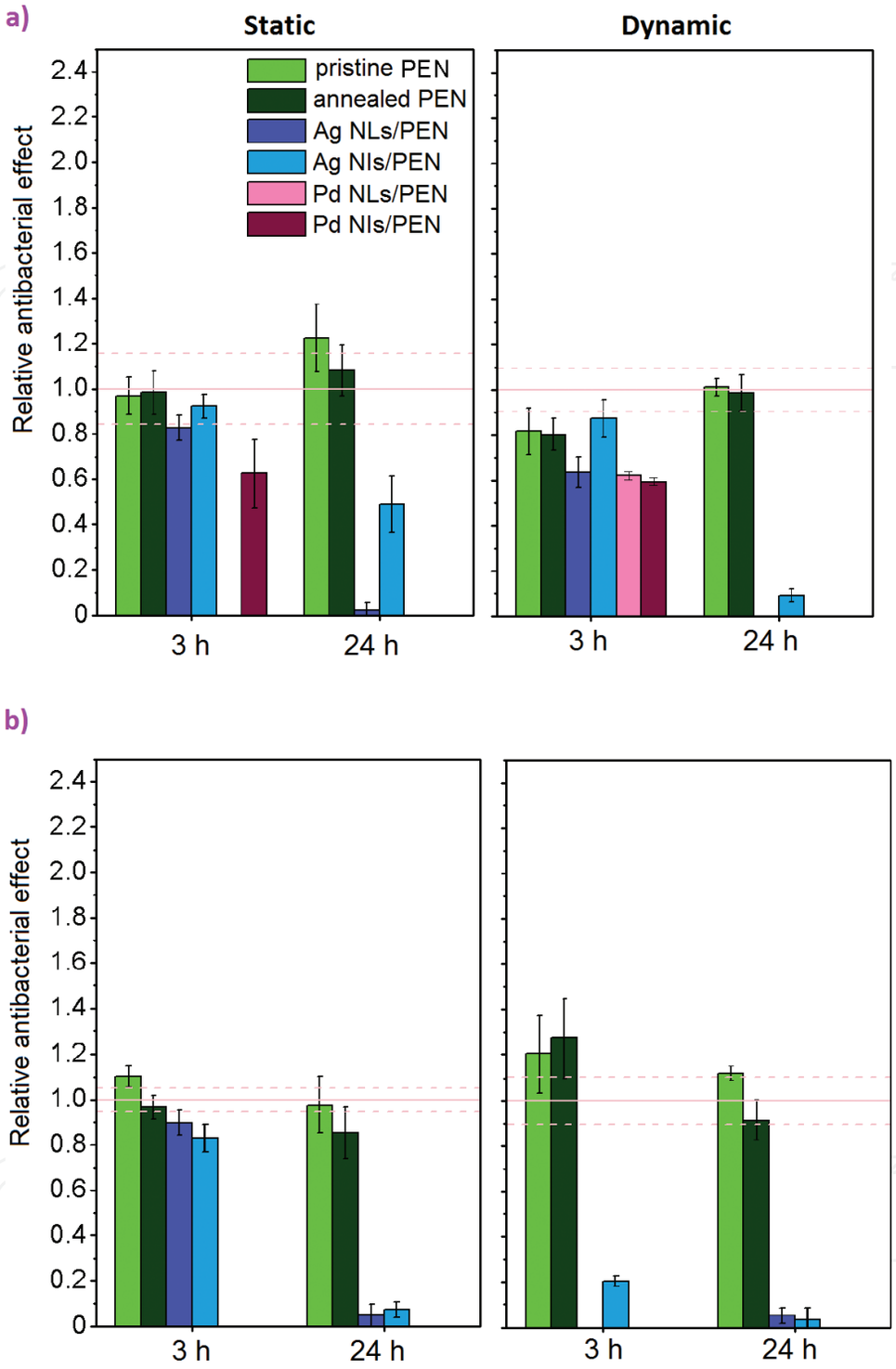

Figure 7. Relative antibacterial effect; number of CFU for examined sample divided by number of CFU for control sample (physiological solution) of the bacterial colonies of (a) *E. coli* and (b) *S. epidermidis* for both, pristine and annealed PEN, Ag and Pd/PEN composites measured in static and dynamic mode. Pink line represents a reference level (number of CFU in physiological solution) for corresponding bacterial strains together with its uncertainty (dash line).

The results for pristine and rippled PEN, Ag NWs/PEN and Pd equivalents are in **Figure 8**. One can see that pristine and rippled PEN were not antibacterial-active in all conditions. The exception is rippled PEN in dynamic mode after 24 h of cultivation of *S. epidermidis*

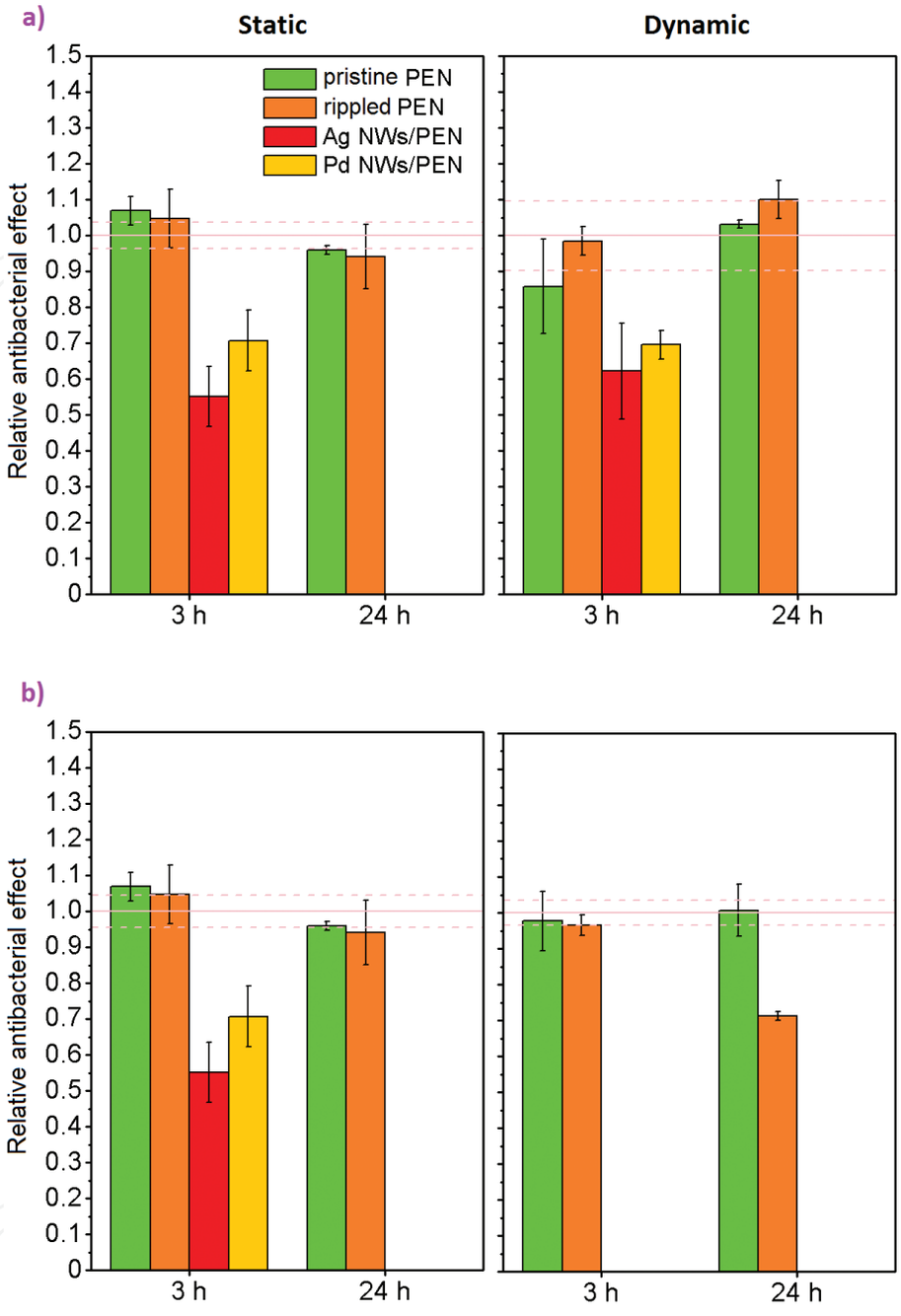

Figure 8. Relative antibacterial effect; number of CFU for examined sample divided by number of CFU for control sample (physiological solution) of the bacterial colonies of (a) *E. coli* and (b) *S. epidermidis* for both, pristine and rippled PEN, Ag and Pd NWs/PEN samples measured in static and dynamic mode. Pink line represents a reference level (number of CFU in physiological solution) for corresponding bacterial strains together with its uncertainty (dash line).

(**Figure 8(b)**). Mild antibacterial effect (ca. 30% of control sample) might be a consequence of higher sensitivity of Gram-positive bacteria to physicochemical and surface properties of a materials, with which they are in a contact, such as hydrophilicity/hydrophobicity, surface charge, presence of some functional groups, and, as in this case, surface morphology and

roughness (see **Figure 6**, AFM) [74, 75]. Antibacterial effect of Ag NWs/PEN and Pd ones samples increase with incubation time in both bacterial strains and both modes. Unlike *E. coli* (**Figure 8(a)**), these samples even exhibited total inhibition (no countable CFUs) after both, 3 and 24 h of incubation of *S. epidermidis* in dynamic conditions (**Figure 8(b)**). The difference between the results of *E. coli* and *S. epidermidis* might be explained by above-mentioned different composition of their cell walls; positively charged particles of noble metals then more facile penetrate through the cell walls of Gram-positive bacteria (*S. epidermidis*) [73]. The samples of Ag and Pd NWs showed comparable antibacterial effects between themselves in case of both bacterial strains, incubation times and modes, which well corresponds with presumed use of Pd NWs as an alternative of the most commonly used Ag in its medical applications as a strongly effective antibacterial agent (antibacterial coatings of catheters and other medical devices) [70–72].

4.5. Cell viability tests

Because the increase of the surface roughness of material (see **Figures 5** and **6** AFM) can, in some cases, lead to its enhanced biocompatibility (adhesion and proliferation of human cells [58, 59]), this paragraph is dedicated to cell viability testing of prepared Ag and Pd composites. Cell viability results for NLs and NIs structures are shown in **Figure 9**, for NWs in **Figure 10**.

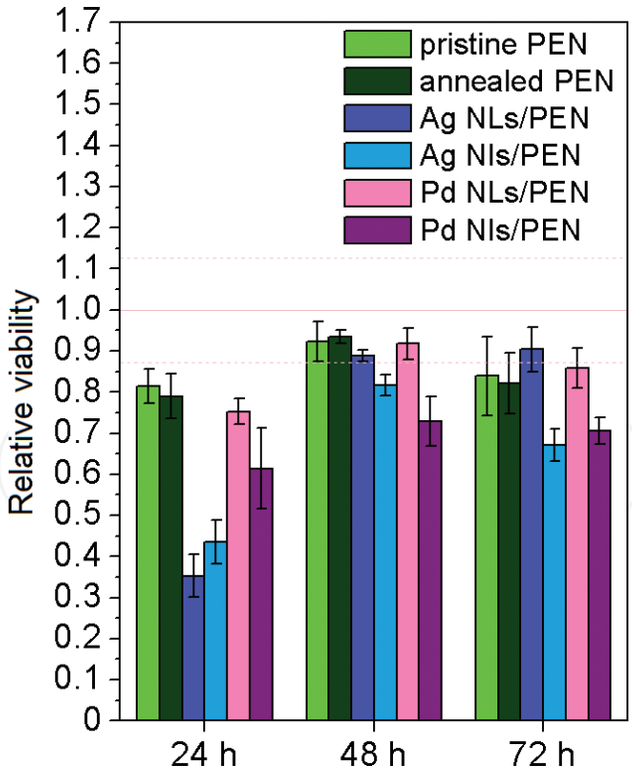

Figure 9. Relative viability; absorbance of examined sample divided by absorbance of control sample (TCPS) of the L929 model cell line for both, pristine and annealed PEN, Ag and Pd/PEN composites. Pink line represents a reference level (absorbance of TCPS) together with its uncertainty (dash line).

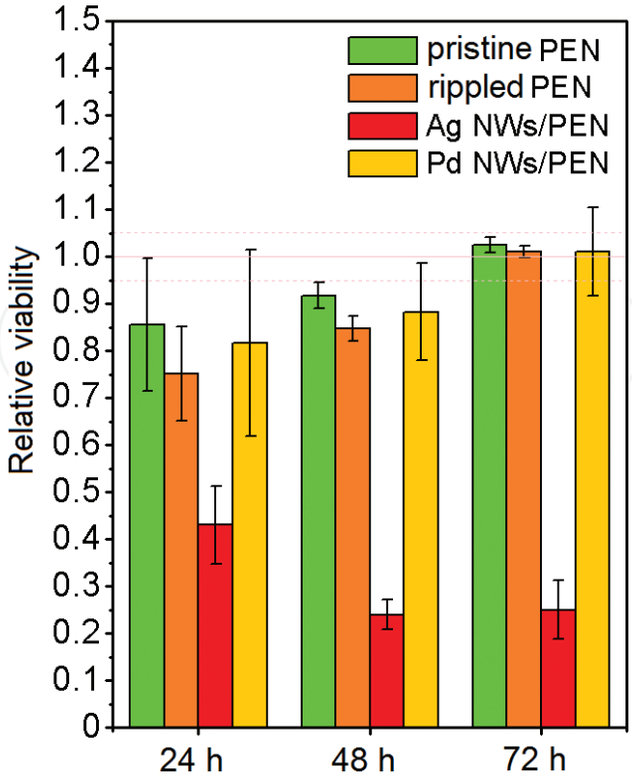

Figure 10. Relative viability; absorbance of examined sample divided by absorbance of control sample (TCPS) of the L929 model cell line for rippled PEN, and Ag and Pd NWs/PEN samples. Pink line represents a reference level (absorbance of TCPS) together with its uncertainty (dash line).

In recent studies, one can observe the references about cytotoxicity of nanostructured metal-based coatings of medical devices to human cells, from which Ag NWs seems to be the most cytotoxic ones [76–78]. Therefore, data from these assays serve as well for safer applications of nanometal/polymer composites in medicine and health-care industry in terms of their cytotoxicity. In following, relative viability of mouse embryonic fibroblasts (L929) was studied by WST-1 cytotoxicity assay [79, 80]. This assay is based on a reduction of tetrazolium salt, which yields water-soluble formazan by oxidoreductases of metabolically active (viable) cells. Formazan is then spectrophotometrically measured at 450 nm. The measured absorbance is directly proportional to the amount of the arisen formazan, which corresponds to the oxidoreductase activity, and thus, to the number of viable cells. Model cell line was cultivated for 24, 48 and 72 h, and acquired absorbance value for examined samples was divided by absorbance value for control sample (standard tissue culture polystyrene, TCPS).

Figure 9 shows the results for pristine and annealed PEN, NLs and NIs/PEN composites, both Ag and Pd. One can see that cell viability on PEN substrate was not changed by annealing and was comparable with control sample (TCPS) after longer cultivation times (48 and 72 h) in case of both, pristine and annealed equivalent. Insignificant decrease of relative cell viability of these samples, as well as the samples of NLs and NIs, both Ag and Pd, after 24 h, is connected with worse adaptation of cell culture after its deployment on the surfaces of the samples; TCPS is a material with optimized properties for *in vitro* cultivation of eukaryotic cells, and therefore, is frequently used as a "gold" cultivation standard [81]. Generally, one can

observe low cytotoxicity of all samples (NLs and NIs ones), where the cell viability on NLs samples (Ag and Pd) was superior. Interestingly, cell viability after longer cultivation times (48 and 72 h) on NLs samples was comparable regardless of the metal used. The same results were observed on NIs; both metals were comparably safe for cells. More significant cytotoxicity of annealed samples (Ag and Pd NIs/PEN) compared to as-sputtered ones (NLs/PEN) was presumably caused by high sensitivity of L929 cell line to rougher surfaces [69], rather than by cytotoxic action of metals; the results of XPS analysis (see **Table 3**) and other results published elsewhere [8] revealed partial covering of metal NIs by thin polymer layer, which decreased the amount of the metals available for cytotoxic action. To sum up, the increase of surface area and roughness in our case (see **Figure 5** AFM) did not led to the enhanced biocompatibility of the samples.

Cell viability results as obtained for pristine and rippled PEN, Ag and Pd NWs/PEN samples are shown in **Figure 10**. After all cultivation times, pristine PEN was not find to be cytotoxic. However, rippled one showed mild cytotoxicity after 24 and 48 h of cultivation of L929 cell line (ca. 15% of TCPS), which disappeared after 72 h. Since L929 cell line is characterized by high sensitivity to rougher surfaces [69], accordingly to previous case of NIs samples, it indicates that the cytotoxic effects were caused by more difficult adaptation and fixation of L929 onto rippled surface of PEN. Cytotoxicity testing confirms significant cytotoxic effects of Ag NWs, reported in a literature [76–78], which was, in the case of ours, determined to more than 50% of TCPS and increased with cultivation time. On the other hand, no cytotoxicity was detected for Pd NWs, in case of all cultivation times. Therefore, these samples could be a safer alternative to Ag NWs ones. Alike in previous case, increased surface area and roughness; induced now by laser patterning and subsequent metal deposition, did not resulted in improved biocompatibility.

5. Conclusions

We have shown that cathode sputtering can be used to prepare NPs of the desired size, which are suitable for subsequent study of their physicochemical properties, since the resulting system is usually composed of only two components; the NPs and the liquid medium used. In particular, sputtering into glycerol is advantageous for detecting of NPs biological properties without the need to consider the surfactant interaction. Results obtained in those systems can be used not only for qualitative research, for example, whether the NPs cytotoxicity is due to ROS induction or dissolution, but also for quantitative determination of toxic dose values.

This chapter also attempted to give comprehensive overview on various kinds of antibacterial-active nanostructured metal coatings of biocompatible PEN potentially applicable in medical devices. Various nanostructures such as NLs, NIs, and NWs were considered and their biological, antibacterial properties and cytotoxic efficacy were broadly discussed. The most commonly used metal in medical and health-care applications (nanostructured Ag) was confronted with Pd. It was found that the increase of surface roughness led to decrease of antibacterial effects of all nanostructured metal/PEN composites; particularly due to so-called ”curtain “ effect in case of NIs ones and biocompatibility, due to relatively high sensitivity

of used L929 cell line to rougher surfaces. The metal-coated samples forming NLs and NIs structures exhibited insignificant cytotoxic effects; taking into account the extent of action, which were presumably caused by increased surface roughness of the samples, rather than by cytotoxic action of nanostructured metal. Generally, the lowest cytotoxicity was found for metal NLs/PEN composites, both Ag and Pd at the same level. The higher antibacterial efficacy of Pd ones, however, predetermines them as a more suitable alternative in medical and health-care applications. Regarding to results of antibacterial and cytotoxicity tests, in case of laser-patterned samples, it turned out that both Ag and Pd NWs/PEN composites have the appropriate antibacterial properties. However, only Pd ones fulfill the condition of cells´ safety, which makes them suitable candidates for the use as antibacterial coatings of medical devices instead of Ag. The potential applications of Ag NWs in medicine and health-care industry are found to be limited and their contact with living tissues, for example, the treatment of medical devices, should be minimized.

Acknowledgements

Financial support of this work from the GACR projects Nos. 17-10907S and P108/12/G108 is gratefully acknowledged.

Author details

Jakub Siegel*, Marek Staszek, Markéta Polívková, Michaela Valová, Pavla Šuláková and Václav Švorčík

*Address all correspondence to: jakub.siegel@vscht.cz

Department of Solid State Engineering, University of Chemistry and Technology Prague, Prague, Czech Republic

References

[1] Polivkova M, Strublova V, Hubacek T, Rimpelova S, Svorcik V, Siegel J. Surface characterization and antibacterial response of silver nanowire arrays supported on laser-treated polyethylene naphthalate. Materials Science and Engineering C: Materials for Biological Applications. 2017;**72**:512-518. DOI: 10.1016/j.msec.2016.11.072

[2] Polivkova M, Siegel J, Rimpelova S, Hubacek T, Kolska Z, Svorcik V. Cytotoxicity of Pd nanostructures supported on PEN: Influence of sterilization on Pd/PEN interface. Materials Science and Engineering C: Materials for Biological Applications. 2017;**70**:479-486. DOI: 10.1016/j.msec.2016.09.032

[3] Polivkova M, Hubacek T, Staszek M, Svorcik V, Siegel J. Antimicrobial treatment of polymeric medical devices by silver nanomaterials and related technology. International Journal of Molecular Sciences. 2017;**18**:1-24. DOI: 10.3390/ijms18020419

[4] Reznickova A, Siegel J, Slavikova N, Kolska Z, Staszek M, Svorcik V. Metal nanoparticles designed PET: Preparation, characterization and biological response. Reactive and Functional Polymers. 2016;**105**:1-8. DOI: 10.1016/j.reactfunctpolym.2016.05.012

[5] Siegel J, Polivkova M, Staszek M, Kolarova K, Rimpelova S, Svorcik V. Nanostructured silver coatings on polyimide and their antibacterial response. Materials Letters. 2015; **145**:87-90. DOI: 10.1016/j.matlet.2015.01.050

[6] Slepicka P, Kasalkova NS, Siegel J, Kolska Z, Bacakova L, Svorcik V. Nano-structured and functionalized surfaces for cytocompatibility improvement and bactericidal action. Biotechnology Advances. 2015;**33**:1120-1129. DOI: 10.1016/j.biotechadv.2015.01.001

[7] Siegel J, Polivkova M, Kasalkova NS, Kolska Z, Svorcik V. Properties of silver nanostructure-coated PTFE and its biocompatibility. Nanoscale Research Letters. 2013;**8**:1-10. DOI: 10.1186/1556-276x-8-388

[8] Polivkova M, Valova M, Siegel J, Rimpelova S, Hubacek T, Lyutakov O, Svorcik V. Antibacterial properties of palladium nanostructures sputtered on polyethylene naphthalate. RSC Advances. 2015;**5**:73767-73774. DOI: 10.1039/c5ra09297c

[9] Staszek M, Siegel J, Rimpelova S, Lyutakov O, Svorcik V. Cytotoxicity of noble metal nanoparticles sputtered into glycerol. Materials Letters. 2015;**158**:351-354. DOI: 10.1016/j.matlet.2015.06.021

[10] Staszek M, Siegel J, Kolarova K, Rimpelova S, Svorcik V. Formation and antibacterial action of Pt and Pd nanoparticles sputtered into liquid. Micro & Nano Letters. 2014;**9**:778-781. DOI: 10.1049/mnl.2014.0345

[11] Siegel J, Kolarova K, Vosmanska V, Rimpelova S, Leitner J, Svorcik V. Antibacterial properties of green-synthesized noble metal nanoparticles. Materials Letters. 2013;**113**:59-62. DOI: 10.1016/j.matlet.2013.09.047

[12] Lyutakov O, Kalachyova Y, Solovyev A, Vytykacova S, Svanda J, Siegel J, Ulbrich P, Svorcik V. One-step preparation of antimicrobial silver nanoparticles in polymer matrix. Journal of Nanoparticle Research. 2015;**17**:1-11. DOI: 10.1007/s11051-015-2935-3

[13] Eid M. Gamma radiation synthesis and characterization of starch based polyelectrolyte hydrogels loaded silver nanoparticles. Journal of Inorganic and Organometallic Polymers and Materials 2011;**21**:297-305. DOI: 10.1007/s10904-010-9448-4

[14] Shervani Z, Yamamoto Y. Carbohydrate-directed synthesis of silver and gold nanoparticles: Effect of the structure of carbohydrates and reducing agents on the size and morphology of the composites. Carbohydrate Research. 2011;**346**:651-658. DOI: 10.1016/j.carres.2011.01.020

[15] Vimala K, Sivudu KS, Mohan YM, Sreedhar B, Raju KM. Controlled silver nanoparticles synthesis in semi-hydrogel networks of poly(acrylamide) and carbohydrates: A rational methodology for antibacterial application. Carbohydrate Polymers. 2009;**75**:463-471. DOI: 10.1016/j.carbpol.2008.08.009

[16] Batabyal SK, Basu C, Das AR, Sanyal GS. Green chemical synthesis of silver nanowires and microfibers using starch. Journal of Biobased Materials and Bioenergy. 2007;**1**:143-147. DOI: 10.1166/jbmb.2007.016

[17] Vosmanska V, Kolarova K, Rimpelova S, Kolska Z, Svorcik V. Antibacterial wound dressing: Plasma treatment effect on chitosan impregnation and in situ synthesis of silver chloride on cellulose surface. RSC Advances. 2015;**5**:17690-17699. DOI: 10.1039/c4ra16296j

[18] Han J, Wang M, Hu Y, Zhou C, Guo R. Conducting polymer-noble metal nanoparticle hybrids: Synthesis mechanism application. Progress in Polymer Science. 2017;**70**:52-91. DOI: 10.1016/j.progpolymsci.2017.04.002

[19] Svorcik V, Kolska Z, Siegel J, Slepicka P. "Short" dithiol and Au nanoparticles grafting on plasma treated polyethyleneterephthalate. Journal of Nano Research. 2013;**25**:40-48. DOI: 10.4028/www.scientific.net/JNanoR.25.40

[20] Siegel J, Lyutakov O, Polívková M, Staszek M, Hubáček T, Švorčík V. Laser-assisted immobilization of colloid silver nanoparticles on polyethyleneterephthalate. Applied Surface Science. 2017;**420**:661-668. DOI: 10.1016/j.apsusc.2017.05.151

[21] Gao-xiang Y, Chun-mu F, Qi-rui Z, Hong-liang G, Xuan-jia Z. Structural and critical behaviors of Ag rough films deposited on liquid substrates. Chinese Physics Letters. 1996;**13**:772. DOI: 10.1088/0256-307X/13/10/016

[22] Borra EF, Seddiki O, Angel R, Eisenstein D, Hickson P, Seddon KR, Worden SP. Deposition of metal films on an ionic liquid as a basis for a lunar telescope. Nature. 2007;**447**:979. DOI: 10.1038/nature05909

[23] Antonietti M, Kuang D, Smarsly B, Zhou Y. Ionic liquids for the convenient synthesis of functional nanoparticles and other inorganic nanostructures. Angewandte Chemie International Edition. 2004;**43**:4988-4992. DOI: 10.1002/anie.200460091

[24] Wender H, Migowski P, Feil AF, Teixeira SR, Dupont J. Sputtering deposition of nanoparticles onto liquid substrates: Recent advances and future trends. Coordination Chemistry Reviews. 2013;**257**:2468-2483. DOI: 10.1016/j.ccr.2013.01.013

[25] Paulechka YU, Kabo GJ, Blokhin AV, Vydrov OA, Magee JW, Frenkel M. Thermodynamic properties of 1-butyl-3-methylimidazolium hexafluorophosphate in the ideal gas state. Journal of Chemical & Engineering Data. 2003;**48**:457-462. DOI: 10.1021/je025591i

[26] Hanusek J. Iontove kapaliny—nový směr v "zelene" chemii. Chemicke Listy. 2005;**99**:265-267

[27] Thuy Pham TP, Cho C-W, Yun Y-S. Environmental fate and toxicity of ionic liquids: A review. Water Research. 2010;**44**:352-372. DOI: 10.1016/j.watres.2009.09.030

[28] Wender H, de Oliveira LF, Feil AF, Lissner E, Migowski P, Meneghetti MR, Teixeira SR, Dupont J. Synthesis of gold nanoparticles in a biocompatible fluid from sputtering deposition onto castor oil. Chemical Communications 2010;**46**:7019-7021. DOI: 10.1039/c0cc01353f

[29] Slepicka P, Elashnikov R, Ulbrich P, Staszek M, Kolska Z, Svorcik V. Stabilization of sputtered gold and silver nanoparticles in PEG colloid solutions. Journal of Nanoparticle Research. 2015;**17**:1-15. DOI: 10.1007/s11051-014-2850-z

[30] Reznickova A, Slepicka P, Slavikova N, Staszek M, Svorcik V. Preparation, aging and temperature stability of PEGylated gold nanoparticles. Colloids and Surfaces A: Physicochemical and Engineering Aspects. 2017;**523**:91-97. DOI: 10.1016/j.colsurfa.2017.04.005

[31] Ndiaye PM, Tavares FW, Dalmolin I, Dariva C, Oliveira D, Oliveira JV. Vapor pressure data of soybean oil, castor oil, and their fatty acid ethyl ester derivatives. Journal of Chemical & Engineering Data. 2005;**50**:330-333. DOI: 10.1021/je049898o

[32] Gref R, Lück M, Quellec P, Marchand M, Dellacherie E, Harnisch S, Blunk T, Müller RH. 'Stealth' corona-core nanoparticles surface modified by polyethylene glycol (PEG): Influences of the corona (PEG chain length and surface density) and of the core composition on phagocytic uptake and plasma protein adsorption. Colloids and Surfaces B: Biointerfaces. 2000;**18**:301-313. DOI: 10.1016/S0927-7765(99)00156-3

[33] Association GP. Physical Properties of Glycerine and its Solutions. Glycerine Producers' Association. New York; 1963

[34] Wender H, de Oliveira LF, Migowski P, Feil AF, Lissner E, Prechtl MH, Teixeira SR, Dupont J. Ionic liquid surface composition controls the size of gold nanoparticles prepared by sputtering deposition. Journal of Physical Chemistry C 2010;**114**:11764-11768. DOI: 10.1021/jp102231x

[35] Hatakeyama Y, Takahashi S, Nishikawa K. Can temperature control the size of Au nanoparticles prepared in ionic liquids by the sputter deposition technique? Journal of Physical Chemistry C. 2010;**114**:11098-11102. DOI: 10.1021/jp102763n

[36] Richter K, Birkner A, Mudring A-V. Stabilizer-free metal nanoparticles and metal–metal oxide Nanocomposites with long-term stability prepared by physical vapor deposition into ionic liquids. Angewandte Chemie International Edition. 2010;**49**:2431-2435. DOI: 10.1002/anie.200901562

[37] Hatakeyama Y, Morita T, Takahashi S, Onishi K, Nishikawa K. Synthesis of gold nanoparticles in liquid polyethylene glycol by sputter deposition and temperature effects on their size and shape. Journal of Physical Chemistry C. 2011;**115**:3279-3285. DOI: 10.1021/jp110455k

[38] Anantha P, Cheng T, Tay YY, Wong CC, Ramanujan RV. Facile production of monodisperse nanoparticles on a liquid surface. Nanoscale. 2015;**7**:16812-16822. DOI: 10.1039/C5NR05904F

[39] Ali M, Abarca G, Eberhardt D, Gual A, Bernardi F, Teixeira SR, Dupont J. "Save money" during hydrogenation reactions by exploiting the superior performance of Pd-NPs deposited on carbon black by magnetron sputtering. Tetrahedron. 2017;**73**:5593-5598. DOI: 10.1016/j.tet.2016.11.043

[40] Staszek M, Siegel J, Polivkova M, Svorcik V. Influence of temperature on silver nanoparticle size prepared by sputtering into PVP-glycerol system. Materials Letters. 2017;**186**:341-344. DOI: 10.1016/j.matlet.2016.10.036

[41] Tsuzuki T. Commercial scale production of inorganic nanoparticles. International Journal of Nanotechnology. 2009;**6**:567-578. DOI: 10.1504/IJNT.2009.024647

[42] Park E-J, Bae E, Yi J, Kim Y, Choi K, Lee SH, Yoon J, Lee BC, Park K. Repeated-dose toxicity and inflammatory responses in mice by oral administration of silver nanoparticles. Environmental Toxicology and Pharmacology. 2010;**30**:162-168. DOI: 10.1016/j.etap.2010.05.004

[43] Lima R, Seabra AB, Durán N. Silver nanoparticles: A brief review of cytotoxicity and genotoxicity of chemically and biogenically synthesized nanoparticles. Journal of Applied Toxicology. 2012;**32**:867-879. DOI: 10.1002/jat.2780

[44] Shukla R, Bansal V, Chaudhary M, Basu A, Bhonde RR, Sastry M. Biocompatibility of gold nanoparticles and their Endocytotic fate inside the cellular compartment: A microscopic overview. Langmuir. 2005;**21**:10644-10654. DOI: 10.1021/la0513712

[45] Pernodet N, Fang X, Sun Y, Bakhtina A, Ramakrishnan A, Sokolov J, Ulman A, Rafailovich M. Adverse effects of citrate/gold nanoparticles on human dermal fibroblasts. Small. 2006;**2**:766-773. DOI: 10.1002/smll.200500492

[46] Asharani PV, Lianwu Y, Gong Z, Valiyaveettil S. Comparison of the toxicity of silver, gold and platinum nanoparticles in developing zebrafish embryos. Nanotoxicology. 2011;**5**:43-54. DOI: 10.3109/17435390.2010.489207

[47] Gao J, Liang G, Zhang B, Kuang Y, Zhang X, Xu B. FePt@CoS_2 Core-Shell Nanocrystals as a potent agent to kill HeLa cells. Journal of the American Chemical Society. 2007;**129**:1428-1433. DOI: 10.1021/ja067785e

[48] Bakri SJ, Pulido JS, Mukherjee P, Marler RJ, Mukhopadhyay D. Absence of histologic retinal toxicity of intravitreal nanogold in a rabbit model. Retina. 2008;**28**:147-149. DOI: 10.1097/IAE.0b013e3180dc9360

[49] Muñoz-Bonilla A, Fernández-García M. Polymeric materials with antimicrobial activity. Progress in Polymer Science. 2012;**37**:281-339. DOI: 10.1016/j.progpolymsci.2011.08.005

[50] Timofeeva L, Kleshcheva N. Antimicrobial polymers: Mechanism of action, factors of activity, and applications. Applied Microbiology and Biotechnology. 2011;**89**:475-492. DOI: 10.1007/s00253-010-2920-9

[51] Tashiro T. Antibacterial and bacterium adsorbing macromolecules. Macromolecular Materials and Engineering. 2001;**286**:63-87. DOI: 10.1002/1439-2054(20010201)286:2<63:AID-MAME63>3.0.CO;2-H

[52] Gabriel GJ, Som A, Madkour AE, Eren T, Tew GN. Infectious disease: Connecting innate immunity to biocidal polymers. Materials Science and Engineering: R: Reports. 2007;**57**:28-64. DOI: 10.1016/j.mser.2007.03.002

[53] Page K, Wilson M, Parkin IP. Antimicrobial surfaces and their potential in reducing the role of the inanimate environment in the incidence of hospital-acquired infections. Journal of Materials Chemistry. 2009;**19**:3819-3831. DOI: 10.1039/b818698g

[54] Roe D, Karandikar B, Bonn-Savage N, Gibbins B, Roullet J-B. Antimicrobial surface functionalization of plastic catheters by silver nanoparticles. The Journal of Antimicrobial Chemotherapy. 2008;**61**:869-876. DOI: 10.1093/jac/dkn034

[55] Yao Y, Ohko Y, Sekiguchi Y, Fujishima A, Kubota Y. Self-sterilization using silicone catheters coated with Ag and TiO2 nanocomposite thin film. Journal of Biomedial Materials Research Part B Applied Biomaterials. 2008;**85**:453-460. DOI: 10.1002/jbm.b.30965

[56] Siegel J, Polívková M, Kasálková NS, Kolská Z, Švorčík V. Properties of silver nanostructure-coated PTFE and its biocompatibility. Nanoscale Research Letters. 2013;**8**:388. DOI: 10.1186/1556-276X-8-388

[57] Siegel J, Krajcar R, Kolská Z, Hnatowicz V, Švorčík V. Annealing of gold nanostructures sputtered on polytetrafluoroethylene. Nanoscale Research Letters. 2011;**6**:588. DOI: 10.1186/1556-276X-6-588

[58] Yeung T, Georges PC, Flanagan LA, Marg B, Ortiz M, Funaki M, Zahir N, Ming W, Weaver V, Janmey PA. Effects of substrate stiffness on cell morphology, cytoskeletal structure, and adhesion. Cytoskeleton. 2005;**60**:24-34. DOI: 10.1002/cm.20041

[59] Rebollar E, Frischauf I, Olbrich M, Peterbauer T, Hering S, Preiner J, Hinterdorfer P, Romanin C, Heitz J. Proliferation of aligned mammalian cells on laser-nanostructured polystyrene. Biomaterials. 2008;**29**:1796-1806. DOI: 10.1016/j.biomaterials.2007.12.039

[60] Belardini A, Larciprete MC, Centini M, Fazio E, Sibilia C, Bertolotti M, Toma A, Chiappe D, de Mongeot FB. Tailored second harmonic generation from self-organized metal nano-wires arrays. Optics Express 2009;**17**:3603-3609. DOI: 10.1364/oe.17.003603

[61] Toma A, Chiappe D, Massabo D, Boragno C, Buatier de Mongeot F. Self-organized metal nanowire arrays with tunable optical anisotropy. Applied Physics Letters. 2008;**93**:163104. DOI: 10.1063/1.3002319

[62] Siegel J, Heitz J, Reznickova A, Svorcik V. Preparation and characterization of fully separated gold nanowire arrays. Applied Surface Science. 2013;**264**:443-447. DOI: 10.1016/j.apsusc.2012.10.041

[63] Siegel J, Heitz J, Švorčík V. Self-organized gold nanostructures on laser patterned PET. Surface and Coating Technology. 2011;**206**:517-521. DOI: 10.1016/j.surfcoat.2011.07.080

[64] Tyler B, Castner D, Ratner B. Regularization: A stable and accurate method for generating depth profiles from angle-dependent XPS data. Surface and Interface Analysis. 1989;**14**:443-450. DOI: 10.1002/sia.740140804

[65] Lewis KB, Ratner BD. Observation of surface rearrangement of polymers using ESCA. Journal of Colloid and Interface Science. 1993;**159**:77-85. DOI: 10.1006/jcis.1993.1299

[66] Tůma J, Lyutakov O, Huttel I, Siegel J, Heitz J, Kalachyova Y, Švorčík V. Silver nanostructures prepared by oriented evaporation on laser-patterned poly (methyl methacrylate). Journal of Materials Science. 2013;**48**:900-905. DOI: 10.1007/s10853-012-6812-5

[67] Rimondini L, Farè S, Brambilla E, Felloni A, Consonni C, Brossa F, Carrassi A. The effect of surface roughness on early in vivo plaque colonization on titanium. Journal of Periodontology. 1997;**68**:556-562. DOI: 10.1902/jop.1997.68.6.556

[68] Herigstad B, Hamilton M, Heersink J. How to optimize the drop plate method for enumerating bacteria. Journal of Microbiological Methods. 2001;**44**:121-129. DOI: 10.1016/S0167-7012(00)00241-4

[69] Taylor RL, Verran J, Lees GC, Ward AP. The influence of substratum topography on bacterial adhesion to polymethyl methacrylate. Journal of Materials Science: Materials in Medicine. 1998;**9**:17-22. DOI: 10.1023/A:1008820313720

[70] Knetsch ML, Koole LH. New strategies in the development of antimicrobial coatings: The example of increasing usage of silver and silver nanoparticles. Polymer. 2011;**3**:340-366. DOI: 10.3390/polym3010340

[71] Leaper DJ. Silver dressings: Their role in wound management. International Wound Journal. 2006;**3**:282-294. DOI: 10.1111/j.1742-481X.2006.00265.x

[72] Tran N, Tran PA. Nanomaterial-based treatments for medical device-associated infections. Chemphyschem. 2012;**13**:2481-2494. DOI: 10.1002/cphc.201200091

[73] Jung WK, Koo HC, Kim KW, Shin S, Kim SH, Park YH. Antibacterial activity and mechanism of action of the silver ion in Staphylococcus Aureus and *Escherichia coli*. Applied and Environmental Microbiology. 2008;**74**:2171-2178. DOI: 10.1128/AEM.02001-07

[74] Gao J, Niklason L, Langer R. Surface hydrolysis of poly (glycolic acid) meshes increases the seeding density of vascular smooth muscle cells. Journal of Biomedical Materials Research. 1998;**42**:417-424. DOI: 10.1002/(SICI)1097-4636(19981205)42:3<417:AID-JBM11>3.0.CO;2-D

[75] Kim SR. Surface modification of poly (tetrafluoroethylene) film by chemical etching, plasma, and ion beam treatments. Journal of Applied Polymer Science. 2000;**77**:1913-1920. DOI: 10.1002/1097-4628(20000829)77:9<1913:Aid-App7>3.0.Co;2-#

[76] Stoehr LC, Gonzalez E, Stampfl A, Casals E, Duschl A, Puntes V, Oostingh GJ. Shape matters: Effects of silver nanospheres and wires on human alveolar epithelial cells. Particle and Fibre Toxicology. 2011;**8**:36. DOI: 10.1186/1743-8977-8-36

[77] Zhang T, Wang L, Chen Q, Chen C. Cytotoxic potential of silver nanoparticles. Yonsei Medical Journal. 2014;**55**:283-291. DOI: 10.3349/ymj.2014.55.2.283

[78] Kim MJ, Shin S. Toxic effects of silver nanoparticles and nanowires on erythrocyte rheology. Food and Chemical Toxicology. 2014;**67**:80-86. DOI: 10.1016/j.fct.2014.02.006

[79] Mosmann T. Rapid colorimetric assay for cellular growth and survival: Application to proliferation and cytotoxicity assays. Journal of Immunological Methods. 1983;**65**:55-63. DOI: 10.1016/0022-1759(83)90303-4

[80] Ishiyama M, Tominaga H, Shiga M, Sasamoto K, Ohkura Y, Ueno K. A combined assay of cell vability and in vitro cytotoxicity with a highly water-soluble tetrazolium salt, neutral red and crystal violet. Biological & Pharmaceutical Bulletin. 1996;**19**:1518-1520. DOI: 10.1248/bpb.19.1518

[81] Peskova V, Kubies D, Hulejova H, Himmlova L. The influence of implant surface properties on cell adhesion and proliferation. Journal of Materials Science: Materials in Medicine. 2007;**18**:465-473. DOI: 10.1007/s10856-007-2006-0

IntechOpen